nature communications

Article

https://doi.org/10.1038/s41467-026-72049-9

Sediment-modulated seafloor residence time controls efficient organic carbon burial in subduction zones

Received: 10 November 2025

Accepted: 30 March 2026

Published online: 02 May 2026

Check for updates

Mengfan Chu[1,2], Kejian Liu[1], Zhirong Cai[3], Troy Rasbury[4], Martin Kölling[5], Matthias Zabel[5], Cecilia McHugh[6], Michael Strasser[7], Ken Ikehara[8] & Rui Bao[1,2]

The subduction organic carbon (OC) flux is closely linked with seafloor sedimentation processes. In hadal trenches, sediment transport and resuspension caused by turbidity events provide rapid feedback of subducting carbon fate to seafloor sedimentation dynamics. Here we demonstrate that sediment sorting creates distinct OC burial patterns in the Japan Trench: Prolonged seafloor residence enables preferential removal of labile OC components and result in a refractory subsurface OC pool. Conversely, rapid sediment burial shortens seafloor residence time and promotes subsurface anaerobic OC degradation. We further suggest that these mechanisms result in at least 37.6% loss of the OC subduction flux in accretionary margins due to early diagenetic and thermal alteration processes, while erosive margins only loss 11% during subduction and preferentially transfer thermally stable OC into subduction zones. Our work bridges surficial depositional regimes and deep carbon transfer, highlighting the need to consider depositional settings when refining subduction zone carbon budgets.

The organic carbon (OC) buried in marine sediments regulates Earth's climate by sequestering atmospheric CO_2 and supplementing the deep carbon reservior[1–3]. The journey of OC from the marine realm to the subduction zones involves complex lateral transport[4,5], aging[6,7], and early diagenetic processes[8–10] that selectively filter the carbon fluxes into the deep Earth. These surficial processes determine the biogeochemical and thermal stability of OC prior to subduction, dictating its ultimate fate in Earth's interior. Quantifying this surface-to-mantle OC connectivity remains a pivotal challenge for deep carbon cycle models[3].

Hadal trenches (>6 km water depth) represent an extreme environment with dynamic OC cycling induced by tectonic forces. As the terminal OC depocenters on Earth's surface, hadal trenches receive OC with complex biogeochemical reactivity shaped by variable sediment transport pathways across the continental margin[11–13]. Episodic turbidity currents drive repeated sediment resuspension[14–16], which extends OC seafloor exposure time and intensifies oxidative degradation of labile components[17,18]. Complex trench morphology forms localized sediment depocenters with distinct sedimentation regimes, where rapid sediment burial enhances anaerobic diagenesis that establishes steep geochemical gradients across subsurface

[1]Frontiers Science Center for Deep Ocean Multispheres and Earth System, Key Laboratory of Marine Chemistry Theory and Technology, Ministry of Education, Ocean University of China, Qingdao, China. [2]Laboratory for Marine Geology, Qingdao Marine Science and Technology Center, Qingdao, China. [3]Department of Geology and Mineralogy, Division of Earth and Planetary Sciences, Graduate School of Science, Kyoto University, Kyoto, Japan. [4]Department of Geosciences, Stony Brook University, New York, NY, USA. [5]MARUM—Center for Marine Environmental Sciences, University of Bremen, Bremen, Germany. [6]Queens College, City University of New York, School of Earth and Environmental Sciences, New York, NY, USA. [7]University of Innsbruck, Institute of Geology, Innsbruck, Austria. [8]National Institute of Advanced Industrial Science and Technology (AIST), Geological Survey of Japan, Institute of Geology and Geoinformation, Ibaraki, Japan. e-mail: baorui@ouc.edu.cn

horizons[10,19,20]. Ultimately, these dynamic processes select the OC components that survive to the subduction zone and fuel the deep carbon cycle.

To elucidate the link between surface sedimentation processes and deep carbon dynamics, we focus on the Japan Trench, a high-energy erosive margin that experiences frequent seismically-triggered turbidity events[21,22]. We integrate stable and radiocarbon isotopes ($\delta^{13}C$, $\Delta^{14}C$) from three critical OC reservoirs in trench bottom waters, surface and subsurface sediments (down to 14 mbsf) to capture the OC transformation processes across the seafloor, subsurface sediment and subduction zone continuum. Our study addresses three objectives: First, to decipher the spatially-varying drivers of early diagenetic processes along the hadal trench axis; second, to compare OC preservation efficiencies under contrasting sedimentation dynamics; and third, to elucidate how seafloor processes constrain the carbon transfer to subduction zones. By bridging depositional regimes and deep carbon fluxes, our results identify hadal trenches as an active interface that modulates carbon burial and transfer within subduction zones.

Results and discussion

Prolonged OC residence at the Japan Trench seafloor induced by sediment resuspension

The carbon isotope signatures of suspended and sedimentary OC in the Japan Trench indicate a predominantly marine origin with minor terrestrial and petrogenic contributions (Fig. 1 & Text S1). The overall broad range of $\Delta^{14}C$ values of sedimentary OC reflect the spatial heterogeneity of the OC sources entering the trench, and a broad spectrum of seafloor residence times after deposition. While the OC derives from vertical particle flux or tectonically-triggered turbidity currents[23,24], the isotopic compositions are profoundly reshaped by pre- and post-depositional degradation. Early diagenetic alteration preferentially removes younger and more labile OC components, resulting in a residual OC pool enriched in older, more refractory material with lower $\Delta^{14}C$ values (Text S1). For instance, surface trench sediments at several sites (M0087, 93 and 94) exhibit depleted $\Delta^{14}C$ value (from −843‰ to −412‰) that exceeds values from sedimentary OC on the trench slope or suspended OC in the water column[23,25] (Fig. 1), indicating prolonged seafloor residence and preferential degradation of labile OC following sediment remobilization at these sites.

The carbon isotope difference between sedimentary and suspended carbon pools is particularly pronounced due to sediment resuspension and prolonged exposure at the seafloor, where suspended OC in trench bottom water shows systematically lower $\delta^{13}C$ and $\Delta^{14}C$ values than both vertically exported marine OC and slope-derived sediments ($\delta^{13}C$ averaged −29.44‰ ± 0.05‰; $\Delta^{14}C$ averaged −866‰ ± 80‰; Fig. 1), diverging markedly from its potential sources (Text S1). This isotopic disparity implies intense degradation within a thick, persistent benthic nepheloid layer, which is featured in tectonically-disturbed Japan Trench[26]. Events like the 2011 Tohoku-oki earthquake demonstrate how seismic shaking amplifies sediment resuspension and oxidative OC degradation for months[16,27]. Within these turbid zones, labile OC compounds are selectively remineralized, leaving ^{14}C-depleted residues preserved in the trench sediments.

Repeated resuspension at the sediment-water interface creates different oxygen exposure times, driving divergent OC degradation patterns between suspended and sedimentary OC. Limited bottom water ventilation and the hydrodynamic isolation caused by trench morphology partially inhibits material exchange between the trench bottom water and the upper water column. Such isolation also promotes repeated degradation within the benthic nepheloid layer, where suspended OC can be reworked multiple times before final deposition. The non-unidirectional OC distribution patterns (Text S2 & Fig. S1) along the trench axis exclude the unidirectional bottom current as the primary control on OC preservation. Instead, turbidity currents orthogonally intersecting the trench may have dominated the OC transport dynamics[28,29]. These episodic, often seismically-triggered sediment flows repeatedly transport particles into the benthic nepheloid layer, intensifying OC degradation during transient suspension phases prior to re-deposition. Coupled with complex trench-fill topography, such progresses create localized depocenters where OC undergoes different extents of seafloor residence. Consequently, the combined effects of hydrodynamic isolation, repeated nepheloid-layer processing, and episodic turbidity-current forcing regulate OC residence times and degradation efficiency.

In essence, the sedimentation dynamic driven by localized turbidity currents and regional depositional settings regulate the OC residence and degradation at the Japan Trench seafloor. Carbon preservation in the Japan Trench is mediated by prolonged seafloor exposure induced by event-driven sediment resuspension, while downslope gravitational processes dictate spatial heterogeneity in degradation hotspots. The influence of sedimentary processes on OC residence highlights the impact of highly-variable sedimentation dynamics (resuspension, sorting, etc.) in the Japan Trench.

Hadal carbon preservation controlled by sediment sorting

To resolve how sedimentation regimes govern OC degradation, we classified Japan Trench sites by flow accumulation area (Fig. 2a), which offers a topographic metric quantifying the area of slope sediment funneled into the trench basins[21]. We divided the trench basin into high sediment input depocenters that bury slope-derived sediments in deep basins (water depth >7.6 km), and low-input sites that located in shallower zones with reduced sediment delivery (see the average flow accumulation areas of the two groups in Fig. 2). This classification does not represent a strict sediment delivery boundary, but rather serves as a practical framework for contrasting depositional settings in the trench. For instance, even within a high-input basin, not all areas necessarily receive uniformly high sediment flux. Nonetheless, compared to sedimentation rates, this approach transcends the spatio-temporally variable turbidity events and thereby emphasizes the role of morphology in OC transport and preservation[30,31]. The order-of-magnitude contrast of flow accumulation between high- and low-input sites (Fig. 2) creates spatially distinct OC diagenetic environments along the Japan Trench, and provides a first-order insight into the role of morphology in governing OC dynamics in the trench.

Low-input sites exhibit OC features of sediment sorting during prolonged seafloor exposure including reduced TOC content and older ^{14}C age (Fig. 2b). Particularly, the medium-grained sediment fraction (20–63 μm) exhibits a relatively low shear stress and is therefore more easily entrained by bottom currents. As a result, this "sortable silt" fraction is prone to repeated deposition-resuspension cycles[32–35], leading to prolonged residence at the sediment-water interface and enhanced exposure to oxic conditions. Consistent with this behavior, this fraction exhibits the most depleted $\delta^{13}C$ signature (Fig. 2b), indicating intensified oxidative degradation and aging of OC associated with repeated sediment-water exchange and lateral transport. These dynamics remove more modern OC in low-input systems than in high-input systems (Fig. 2c, see "Method" for interpretation), leading to preservation of a more refractory sedimentary OC pool.

Conversely, the conventional grain-size control on OC preservation is not always applicable in high-input regions. The coarse fraction (> 63 μm) preserves more OC than the finer fraction (< 20 μm, Fig. 2b) despite the fact that fine-fraction sediments generally retain abundant OC[4,6]. This reflects rapid turbidity-driven burial that sequesters coarse particles before oxidative OC degradation occurs, while the fine particles remain trapped in suspension clouds. Higher $\Delta^{14}C$ disparities between suspended and sedimentary OC (Table S1) at the high-input sites also indicate that sedimentary OC in these regions is rapidly buried before significant intra-fraction $\Delta^{14}C$ differences can develop,

https://doi.org/10.1038/s41467-026-72049-9

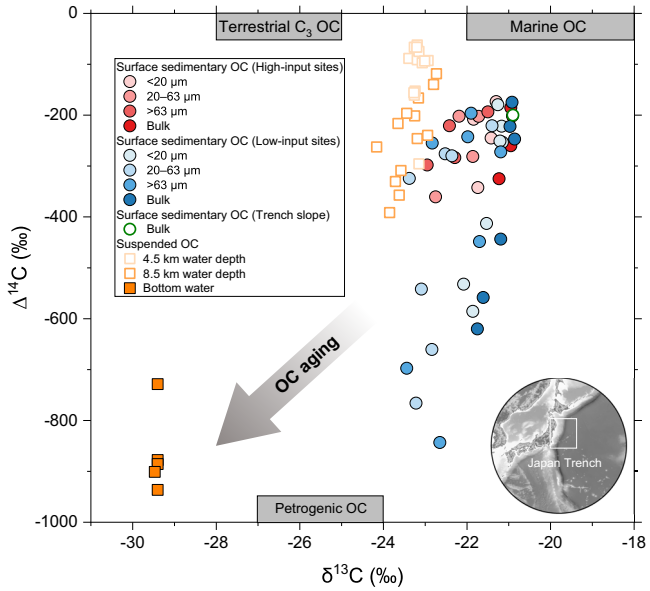


Fig. 1 | Isotopic signatures of suspended and sedimentary organic carbon (OC) in the Japan Trench. Carbon isotope characteristics (^{13}C and ^{14}C) of suspended (solid and open rectangles, from this study and ref. 23., respectively) and surface sedimentary OC at the Japan Trench seafloor (circles for high- and low-input sites, respectively, this study), as well as sedimentary OC at the trench slope (open circle, ref. 74.), plotted with reference endmembers. For three bottom water suspended OC samples lacking $\delta^{13}C$ values, the mean $\delta^{13}C$ of the other two samples was used. All surface sediment samples were taken within the top 3 cm of the retrieved pilot cores. Bathymetric data of the inserted map is derived from the SRTM15+ global relief model[76] and visualized using the Generic Mapping Tools[77](GMT).

whereas suspended OC undergoes prolonged residence in the benthic nepheloid layer (Text S3).

Basin morphology also modulates OC fate through regulating sediment input. Thick turbidite muds, which characteristically contained aggregates of clay particles, can be deposited by ponding of highly sediment-concentrated bottom waters following major earthquakes[36,37]. Such ponding depends not only on the supply of sediment but also on basin geometry and slope morphology. For example, Site M0090 locates in a small and shallow basin, which limits the formation of thick ponded mud layers, resulting in relatively thinner turbidites compared to the deeper Site M0083 (Fig. S2) and lower sediment input (Fig. 2a). While the low-input sites exhibit conventional pattern where the <20 μm fraction particles account for most of the sediment specific surface area (SSA), the coarser fractions show more influence on the SSA in high-input sites (Text S4). This implies that basin size, connectivity, and morphology exert a critical control on the mineral protection and the subsequent burial of OC.

Together, these contrasts highlight sediment input regime and trench morphology as the primary controllers of carbon cycling in the trench. Low-input settings act as oxidative filters where resuspension cycles selectively mineralize labile OC, while high-input zones function as a rapid transfer pathway that preserve diverse OC components. It should be noted that both pathways are tectonically mediated: rapid sediment deposition can dominate the early stage of a turbidity flow, followed by a period of sediment stasis and extended OC residence in the nepheloid layers[38,39] that allows for bioturbation in the top of event deposit[40]. The role of local morphology in shaping deposition and residence time further emphasizes the importance of integrating both input and geomorphological context when assessing OC fate in tectonically-active hadal trenches. This sedimentological filtering should be considered to accurately quantify carbon burial flux in the hadal trenches.

Impact of surface sedimentation dynamics on subsurface carbon cycling

We next investigate how the contrasting depositional settings influence OC degradation during subsurface burial in the trench. By exploiting the CE 869 Jogan Earthquake deposit as a chronostratigraphic marker[38] (Fig. S2 & Text S5), we trace the evolution of the OC pool over 1,152 years of burial (CE 869 to CE 2021). The decrease of modern OC content (Fig. S2) in high-input regions indicates stronger subsurface degradation (11.5% modern OC loss vs. 7.5% in low-input systems, see Method for calculation), in contrast to their preservation advantage at the seafloor. On the other hand, prolonged seafloor exposure at low-input sites pre-ages OC, leaving refractory fractions that are less degradable by organoclastic sulfate reduction upon burial. Lower OC degradation rate in the low-input regions, despite comparable burial durations, is further confirmed by porewater sulfate and alkalinity profiles (Text S6). Specifically, high-input sites show a more rapid increase in alkalinity relative to sulfate consumption, consistent with enhanced organoclastic sulfate reduction, which generates more alkalinity per mole of sulfate reduced than anaerobic oxidation of methane in such depth. This steeper alkalinity-to-sulfate gradient reflects a stronger contribution of organoclastic sulfate reduction and thus more intensive OC mineralization in the subsurface at high-input sites. In contrast, the muted alkalinity production relative to sulfate drawdown at low-input sites indicates weaker organoclastic sulfate reduction, consistent with the predominance of refractory OC that is less susceptible to microbial degradation. In addition, reaction-transport modeling simulations yield substantially lower total OC degradation rates in low-input regions compared to high-input regions[41]. The consistently lower degradation rates at low-input sites support the interpretation that reduced OC reactivity limits subsurface OC degradation in these settings.

In tectonically active hadal trenches, such decoupling mechanism generates a series of carbon cycling processes including instant burial of labile OC component, extended oxidative degradation of suspended OC during gradual settling, and subsurface reactivation of buried OC. This creates a highly dynamic trench carbon cycle shaped by mass-wasting events[42]. Furthermore, the sedimentation-controlled dynamics partition carbon among distinct reservoirs in the trench. In low-input regions, the degradation products are released to the water column during extended seafloor residence cycles (Fig. 3a). Conversely, rapid sediment burial in high-input zones transfers reactive OC to subsurface realms, supplementing porewater dissolved organic and inorganic carbon reservoirs through accelerated anaerobic transformations. The carbon partitioning during burial mediated by event-driven sedimentation creates depth-dependent OC reactivity that further determines the turnover time of the OC in trench.

Large earthquakes can induce rapid shifts of the seafloor morphology, followed by transient depositional processes lasting for months[39]. Our findings thus highlight the need for incorporating hydrodynamic context and OC diagenetic history for accurate understanding the carbon cycling in such systems. Our ^{14}C measurements also reveal that episodic seafloor perturbations and post-depositional processes can introduce significant inter-fraction age offsets. These biases, if unrecognized, may distort age model construction in carbonate-poor sediments[43–45] and impede carbon flux estimation.

As one of the most seismically active hadal trenches worldwide, the Japan Trench recieves a sediment delivery that is overwhelmingly dominated by earthquake-triggered turbidity currents[46–48]. Episodic seismic events thus control sediment accumulation along the trench axis. OC input associated with background hemipelagic sedimentation is several orders of magnitude lower[24], highlighting the dominant role of event-driven sediment transfer in shaping the trench sedimentary environment. This tectonically modulated sediment supply provides a unique natural setting to investigate how episodic sedimentation governs the fate of OC in hadal systems. The large volumes of OC

https://doi.org/10.1038/s41467-026-72049-9

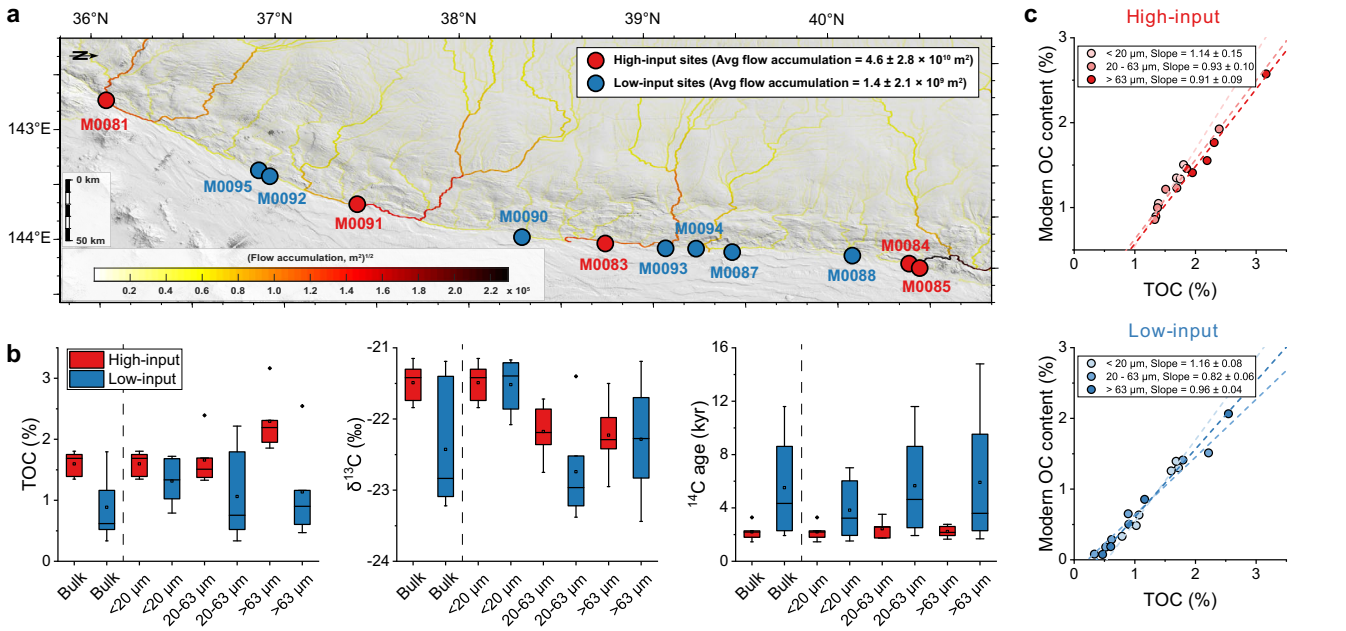


Fig. 2 | Map of the Japan Trench and comparison of organic carbon (OC) characteristics between high- and low input regions. a The map of sediment flow accumulation in the Japan Trench[38], with the high- and low-input sites indicated by color. Flow accumulation is modeled for each depocenters and presented as square root for better contrast by color. **b** Box plots of bulk and grain-size-specific variations in total OC content (TOC), $\delta^{13}C$ values and ^{14}C ages of surface sedimentary OC in high- and low-input sites. The box contains 3/4 of dataset, with the whiskers mark the 5th and 95th percentiles. Values beyond these upper and lower bounds are marked with dots. **c** Covariation between modern (OC% × Fraction modern) and TOC in high- and low-input regions. Smaller slope of the regression line (e.g., in the low-input region) indicates OC degradation during prolonged seafloor residence[71].

episodically transferred into the trench by seismic events are subject to transformation within the trench's unique depositional and hydrodynamic environment. For example, recent work implies that trench morphology and localized circulation can modulate carbon cycling processes in near-bottom waters[49]. Furthermore, carbon transformations occurring at the water-sediment interface regulate both the quantity and reactivity of OC transferred to deeper sediment layers, which in turn control microbially mediated carbon cycling in subsurface sediments[19,50].

Together, these studies emphasized an active trench biogeochemical environment where OC undergoes significant alteration before long-term burial. However, without quantitatively linking depositional regimes to subsequent subsurface OC degradation and long-term burial efficiency, the extent to which surface sedimentation dynamics ultimately regulate carbon fluxes into subduction zones has remained unresolved. The present study advances these earlier efforts by providing a process-based framework that directly links surface depositional regimes to subsurface OC degradation and preservation. This conceptual bridge extends the perspective of trench carbon cycling from surface accumulation to deep burial and enables estimation of how contrasting sedimentation scenarios modulate the magnitude and composition of carbon ultimately entering subduction zones.

The tectonic filter on subduction zone carbon fluxes

Surface sedimentation dynamics may further regulate the thermal vulnerability of the subducting carbon pool by modulating the composition of OC delivered to depth, particularly the relative proportions of thermally labile versus refractory components, which directly determine how much OC is susceptible to early thermal transformation during subduction. Ramped pyrolysis-oxidation analysis of Japan Trench sediments reveals three distinct OC fractions with varying thermal stabilities (Fig. S6). The thermal fraction that decomposes at lowest temperature (C_1 at <200 °C), which is often enriched in labile OC components like cellulose[51–53], is more abundant in the high-input sites (8.2% of total OC versus 3.8% in low-input systems, Fig. S7). This temperature threshold corresponds to ~20 km subduction depth at the Japan Trench[54], where compounds with low thermochemical stability undergo rapid transformation as temperature increases. Moreover, refractory OC can become progressively more reactive during burial, as increasing temperature and pressure alter molecular structures and weaken protective associations with minerals. Such burial-induced activation enhances the susceptibility of previously preserved OC to thermochemical and microbial degradation[55]. High-input environments thus have the potential to shuttle substantial thermally vulnerable carbon into subduction zone, amplifying the spatial heterogeneity in deep carbon fluxes[3,56].

On global scale, the carbon budget of subduction zones is largely governed by the amount and nature of sediment delivered to the trench and the thermal structure of the forearc. Sediment supply also plays a first-order role in controlling the accretionary versus erosive characters of convergent margins. We present a conceptual framework designed to quantify how much of the deposited OC is transformed prior to subduction under different sedimentation regimes, emphasizing depositional and early diagenetic processes within the trench in disregard of OC sources prior to trench delivery. Large sediment input typically promotes accretionary wedge growth, whereas sediment-starved systems tend toward forearc erosion[57,58]. Accretion, and the tendency of accretionary margins to have steeper forearc geothermal gradients[48], promote thermal alteration of OC[3]. The accretionary setting shows similarity with our high-input trench scenario with enhanced sediment input, rapid burial of labile carbon components and intensive carbon alteration in the subsurface (Fig. 3). Conversely, sediment-starved erosive margins receive smaller but more refractory OC fluxes. Although some erosive margins may experience high surface productivity (e.g., the Peru-Chile and Japan Trenches[59–61]), the overall sediment flux delivered to the trench is typically low. In such settings, even if substantial phytoplankton-derived OC is produced, these surface-derived OC undergoes prolonged exposure at the

https://doi.org/10.1038/s41467-026-72049-9

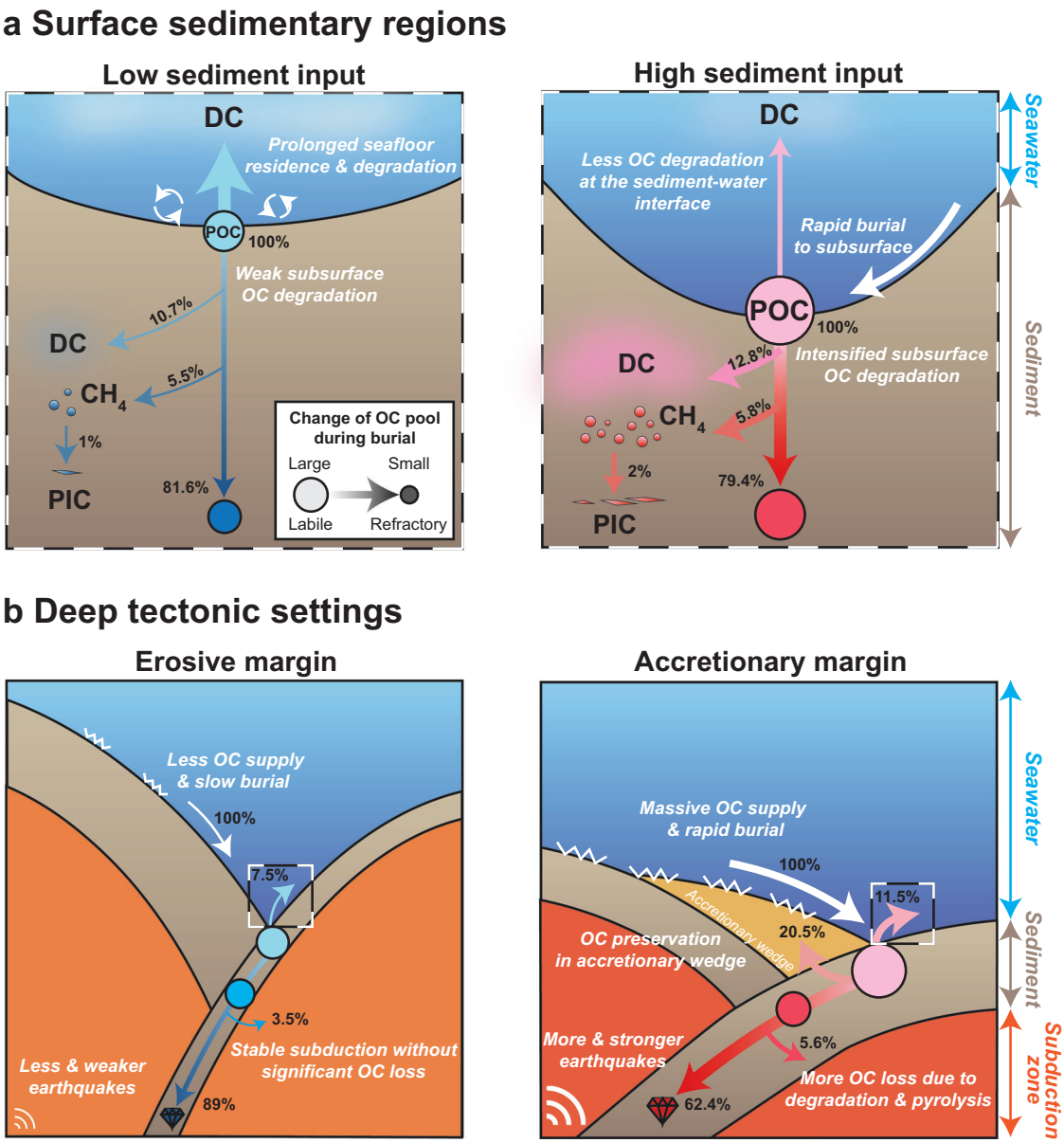


Fig. 3 | Conceptual model illustrating the organic carbon (OC) degradation, pyrolysis and subduction from the seafloor to subduction zone. a OC degradation and burial processes in surface sedimentary regions. In low sediment input scenario, sediment resuspension enhances particulate OC (POC) degradation at the seafloor, leaving less production of dissolved carbon (DC), methane (CH_4) and particulate inorganic carbon (PIC) in the subsurface, and ultimately favoring carbon subduction. Conversely, large amounts of POC are buried with limited degradation at the seafloor in high sediment input scenario, but undergoes intensive degradation in the subsurface. The proportions of carbon fluxes are calculated by results of a reactive transport model[41]. **b** OC pyrolysis and subduction processes in deep tectonic settings. In sediment-starved erosive margins, relatively low sediment discharge result in smaller OC fluxes (indicated by width of arrows) but favors larger OC subduction proportion (indicated by figures) to deeper depths. In accretionary margins, high sediment discharge supply massive labile OC into the trench, leading to overall lower OC subduction proportion despite the high degradation, accretion and pyrolysis OC fluxes. The proportions of carbon fluxes are calculated by the summaries in Table 1.

seafloor, promoting extensive oxidative degradation and thereby limiting the fraction of labile OC that can be buried into deeper sediment layers. Thus, differences in OC source (e.g., surface-derived versus laterally transported) are ultimately filtered by the sedimentation regime, which governs residence time and early diagenetic alteration prior to subduction. In summary, limited burial, as conceptually represented by our low-input trench scenario where prolonged seafloor exposure selectively preserves refractory fractions, restrain OC degradation to the seafloor, allowing stable organic compounds to transit deeper (Fig. 3).

Compared to the fate of inorganic carbon, the global subduction dynamics of OC remain less constrained[62,63]. Surface sediment OC content is often used to approximate the OC subduction flux[56] assuming minor alteration prior to subduction. Our findings demand recalibration of global subducting carbon budgets, as conventional flux models underestimate OC transformation during sedimentary transit. Our quantification using the "high-input" and "low input" as a conceptual model for accretionary and erosive margins, respectively, shows that accretionary systems lose ~37.6% of trench-delivered carbon through early diagenesis and thermal alteration before deep subduction (Table 1). At accretionary margins, despite high sediment input leading to elevated OC delivery to the trench, a significant fraction of this OC may be lost to early degradation and pyrolazation during burial (11.5% and 5.6%, respectively, Fig. 4 & Table 1). In comparison, erosive margins exhibit inverse efficiency, with smaller initial carbon flux yielding proportionally greater deep transfer due to enrichment of refractory

Table 1 | Organic carbon (OC) budget in Pacific subduction zones

Subduction zone	OC Delivered to Trench [a] (Mt/yr)	Accretion Efficiency [a] (%)	OC Degraded (Mt/yr)	OC stored in accretionary wedge (Mt/yr)	OC pyrolyzed (Mt/yr)	OC subducted (Mt/yr)
Erosive margin						
North Chile	0.550	0	0.041	0	0.019	0.489
Peru	0.530	0	0.040	0	0.019	0.472
Colombia-Ecuador	0.271	0	0.020	0	0.010	0.241
Costa Rica	0.083	0	0.006	0	0.003	0.074
Nicaragua	0.037	0	0.003	0	0.001	0.033
Guatemala	0.152	0	0.011	0	0.005	0.135
Mexico	0.252	0	0.019	0	0.009	0.224
Kurile	0.150	0	0.011	0	0.005	0.133
Kamchatka	0.219	0	0.016	0	0.008	0.195
Northeast Japan	0.392	0	0.029	0	0.014	0.349
Izu-Bonin	0.058	0	0.004	0	0.002	0.052
Mariana	0.036	0	0.003	0	0.001	0.032
Ryukyu	0.014	0	0.001	0	0.000	0.012
South Luzon	0.018	0	0.001	0	0.001	0.016
Philippine-Mindanao	0.011	0	0.001	0	0.000	0.010
Solomons	0.246	0	0.018	0	0.009	0.219
Tonga	0.091	0	0.007	0	0.003	0.081
Kermadec	0.167	0	0.013	0	0.006	0.149
Sum	3.277	/	0.246	0	0.115	2.916
Accretionary margin						
South Chile	0.391	16.5	0.045	0.057	0.024	0.265
Oregon-Washington	0.329	20.8	0.038	0.061	0.019	0.212
British Columbia	0.295	16.3	0.034	0.043	0.018	0.201
Alaska	2.096	17.9	0.241	0.332	0.125	1.398
Aleutians	0.728	7.4	0.084	0.048	0.049	0.548
Nankai Trough	0.645	37.0	0.074	0.211	0.029	0.330
Taiwan-North Luzon	0.536	58.6	0.062	0.278	0.016	0.180
Sum	5.020	/	0.577	1.029	0.280	3.134

See "Methods" for OC flux calculations.
[a]OC delivery flux and accretion efficiency are from ref. 56.

components (with only 11% losses to early degradation and pyrolazation, Fig. 4 & Table 1). In erosive setting, a larger proportion of trench-delivered OC is preserved and incorporated into the subducting slab, making the OC subduction efficiency comparably higher (89% in erosive margions comparing to 62.5% in accretionary margins) despite a smaller total flux[56] (Table 1).

After acounting for the OC loss prior to subduction, the difference of OC subduction fluxes is less than that of OC input fluxes between accretionary and erosive margins. These distinctions underscore the need of a subduction flux model that accounts for pre-subduction degradation modulated by seafloor residence time, OC thermal lability governed by depositional regimes, as well as tectonically-driven partitioning between shallow and deep carbon reservoirs. Instead of discriminate between OC sources (i.e., inputs associated with productivity or turbidity events), this model captures the net depositional outcome that regulates the extent of OC alteration prior to subduction. By focusing on depositional dynamics within the trench, we isolate sedimentation-controlled burial efficiency as a higher-order regulator that modulates source variability into measurable differences in degradation intensity prior to subduction.

Ultimately, hadal trenches emerge as reactive filters of Earth's subducting carbon. Surface transient processes at the trench floor like turbidity currents creates pulsed burial events that cascade through subsurface and subduction systems, profoundly modulating OC fate and representing a geological feedbacks to plate subduction. The varying contribution of organic components to the total subduction carbon flux among accretionary and erosive settings may further result in spatial variation of manle composition. Future modeling should integrate these sedimentological filters with reaction kinetics to resolve how episodic deposition shapes the spatial and temporal varying deep carbon cycling. Such advances will position trenches as dynamic regulators in Earth's carbon-climate system and sensitive recorders of geological disturbances.

Methods

Research area

The Japan Trench is a convergent margin where the Pacific plate subducts beneath the Okhotsk plate with a convergence rate of 80–86 mm/yr[64]. It is ~700 km long and ~200 km east of the Japan coastline[65]. Water depths at the trench floor are ~6.8 km in the northern part of the trench and increase southward to more than 8 km[47,66]. The Ogawara and Nakaminato canyons connect the Japan Trench with the continental shelf in the northern and southern trench, respectively. Although these canyon systems may facilitate limited downslope

https://doi.org/10.1038/s41467-026-72049-9

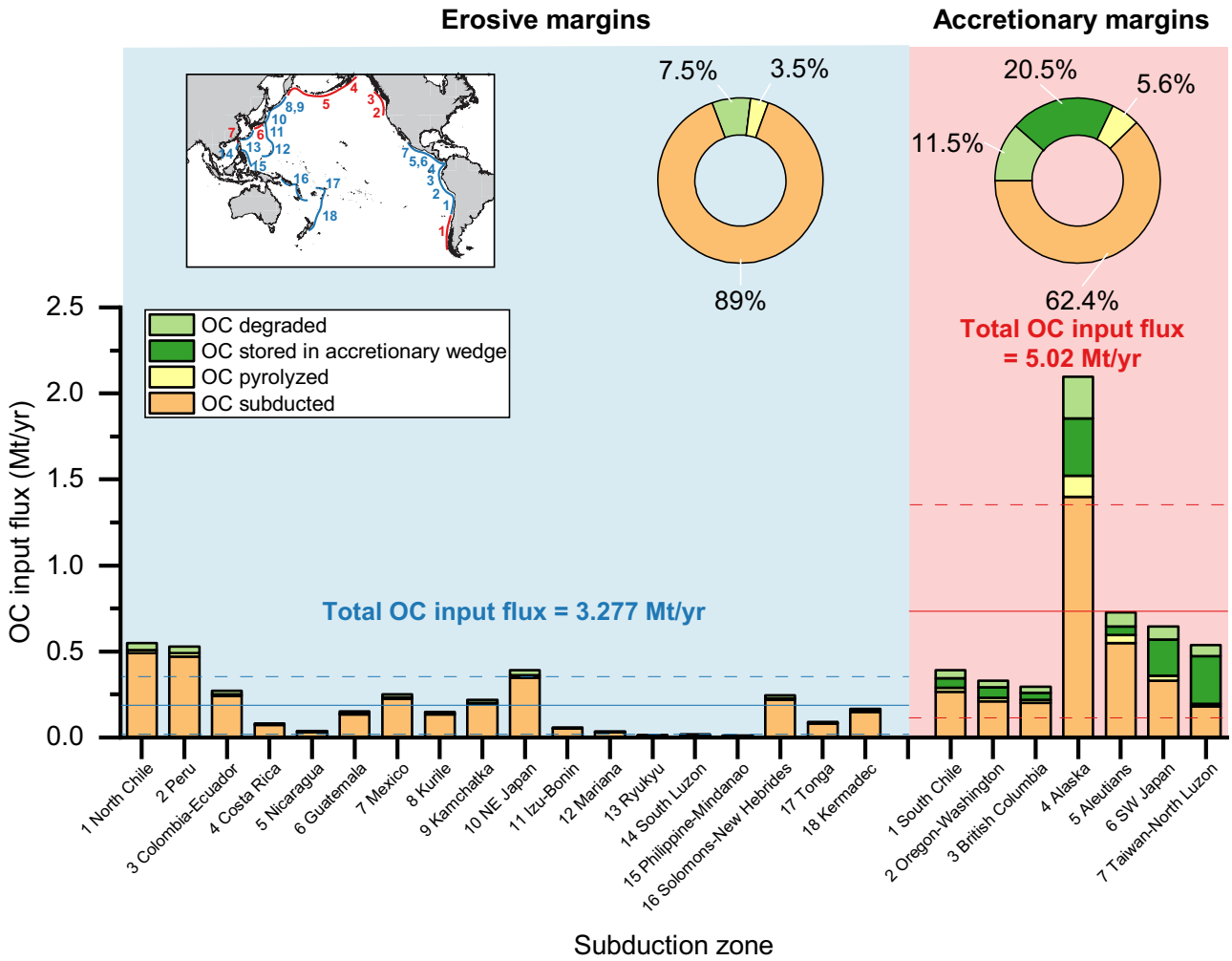


Fig. 4 | Estimated organic carbon (OC) fluxes in the Pacific subduction zones. The OC input fluxes are compiled from ref. 56, with solid and dashed lines indicating average and standard deviation, respectively. The proportions of OC degraded, stored in accretionary wedge, pyrolyzed and subducted are calculated in this study. The map is created with Ocean Data View[78].

gravity-driven sediment transport during periods of reduced seismic activity, they have not been reported as major sediment-routing pathways to the trench floor, rendering seismically induced turbidity currents as the major sediment input pathway in the Japan Trench[21,47,48]. Accordingly, background gravitational transport is likely overwhelmed by episodic earthquake-triggered mass-wasting events. Active bending-related deformation of the subducting oceanic plate results in semi-isolated trench basins formed in horst-and-graben structures along the trench axis[67], with typical vertical relief of a few hundreds of meters. These basins serve as an ideal location for sediment accumulation, effectively trapping sediments delivered by turbidites at the trench floor. The sedimentation rate in the Japan Trench is relatively high (100–400 cm/kyr[66]) due to frequent seismic events in the subduction zone[42], while the average background sedimentation rates (i.e., approximated hemipelagic sedimentation) ranges between 80–300 cm/kyr in the central Japan trench[66] with an average around 225 cm/kyr[38].

Sample collection

Sediment samples were collected on R/V *Kaimei* during the International Ocean Discovery Program (IODP) Expedition 386 in 2021. Surface sediment samples were taken from the top 2 cm of the pilot cores (top 3 cm for Core M0094B), while subsurface sediment samples were taken from giant piston cores at 2 cm intervals (Table S2). Suspended OC was filtered through a pre-combusted GF/F filter from 1 L bottom water sample which was added with 1 mL 10% HCl. All samples are stored at −20°C before analysis. It should be noted that the giant piston core records (e.g., the depth framework in Fig. S2) may lack the uppermost sediment layers due to core recovery limitations as discussed in ref. 38,68. Therefore, aligning pilot core data (used for surface sedimentary OC) with piston core stratigraphy does not reflect the true absolute depth scale. However, since our analysis focuses on relative age differences between surface and subsurface sedimentary OC without considering depth-related sedimentation rate, these depth uncertainties do not affect the interpretation of OC aging patterns.

Mineral specific surface area analysis

The mineral specific surface area (SSA) of bulk sediment samples was determined using a Brunauer-Emmett-Teller (BET) technique on a Micromeritics ASAP 2460 surface area analyzer at Qingdao Institute of Bioenergy and Bioprocess Technology, Chinese Academy of Sciences. Prior to analysis, samples were pre-combusted at 350 °C for 12 hours to remove organic matter. SSA was calculated from N_2 adsorption data using a five-point BET method.

Total organic carbon content and isotopic analysis

Sediment samples were separated into different grain-size fractions (< 20 μm, 20–63 μm, >63 μm) by wet sieving. Bulk sediments were passed through a series of stainless-steel sieves (63 μm and 20 μm

mesh sizes, Retsch GmbH, Germany) under continuous rinsing with Milli-Q water[69]. The >63 μm and 20–63 μm fractions were washed off the sieves with Milli-Q water, while the <20 μm fraction was collected from the filtrate. All fractions were obtained as slurries, subsequently freeze-dried, and homogenized prior to geochemical analyses.

For sedimentary OC, acid fumigation was used as the pretreatment method for carbon content and isotopic analyses. Samples were HCl-fumigated at 60 °C for 72 h, followed by NaOH-fumigated at 60 °C for 72 h to neutralize the excess acid. TOC contents were measured by an elemental analyzer at Ocean University of China. The Elemental Technology Co. Ltd. reference material IVA33802180 was used as a routine working standard for carbon content determination of sediment samples. Samples were weighed into tin capsules before introduction into the EA. The single combustion/reduction reactor of the EA was maintained at 980°C, with the helium flow at 180 mL/min and the oxygen flow at 250 mL/min, and an O_2 injection end time of 5 s. $\delta^{13}C$ values were measured by an isotope ratio mass spectrometer at the National Ocean Sciences Accelerator Mass Spectrometry Facility (NOSAMS), Woods Hole Oceanographic Institution, and are reported relative to Peedee Belemnite. Samples were weighed into tin capsules and combusted in the EA at 1025 °C. The generated CO_2 was then trapped and separated from the helium carrier gas. Approximately 7% of the gas was taken for $\delta^{13}C$ measurement via an isotope ratio mass spectrometer. The remaining gas was reduced with H_2 to graphite and was taken for ^{14}C measurement via an accelerator mass spectrometer by standard procedures at NOSAMS[70]. OX-I normalizing standards and secondary standards including IAEA C-2 and OX-II were routinely run at NOSAMS to estimate the measurement precision and accuracy of the instrument[70].

Effect of hydrodynamic sorting on the modern OC content

Assuming that total sedimentary OC is composed of two components: petrogenic (OC_{petro}) and modern OC (OC_{modern}), when use Fraction modern (Fm) to represent the ratio of the ^{14}C content in a sample to that of the modern standard, OC_{petro} has a Fm = 0 while OC_{modern} has Fm > 0. The mixing of these two endmembers can thus be described by the mass-balance equation:

$$Fm = OC_{modern}\%/OC\% \times Fm_{OCmodern} + OC_{petro}\%/OC\% \times Fm_{OCpetro} \quad (1)$$

Where OC% is the total concentration of OC in the sample (expressed as % of dry weight), OC_{modern}% and $Fm_{OCmodern}$ are the content and radiocarbon composition of modern OC in the sample, respectively; OC_{petro}% and $Fm_{OCpetro}$ are the content and radiocarbon composition of petrogenic OC in the sample, respectively.

Because OC_{petro} is derived from ancient sedimentary rocks and is thus radiocarbon dead, the Fm of the sample is therefore only determined by OC_{modern}:

$$Fm = OC_{modern}\%/OC\% \times Fm_{OCmodern} \quad (2)$$

In terms of OC content, the total OC% is composed of OC_{modern}% and OC_{petro}%:

$$OC_{petro}\% = OC\% - OC_{modern}\% \quad (3)$$

Combining Eqs. (2) and (3) we have:

$$OC\% \times Fm = OC\% \times Fm_{OCrecent} - (OC_{petro}\% \times Fm_{OCrecent}) \quad (4)$$

Where OC% × Fm represents the modern OC content in the sample. When plotting modern (OC% × Fm) against total OC content (OC%), the slope of each regression reflects the selective loss of young, modern OC components, with smaller slope values indicating stronger degradation during repeated sediment resuspension[71]. In this study, we grouped all sites into high- and low-input categories, and performed separate regressions for each grain-size fraction of the surface sediments to assess the extent of OC degradation under different depositional settings and hydrodynamic regimes (Fig. 2c).

Carbon degradation estimation in subsurface sediments

Assuming that the modern (radiocarbon-active) fraction of OC represents the more labile component that is preferentially degraded during burial, we applied a degradation correction factor derived from measurements in the Japan Trench to estimate OC loss via early degradation. At the chosen five sites in the Japan Trench, modern OC content in subsurface sediments is lower than that in surface sediments, indicating substantial OC degradation during burial in both high- and low-input regions. Given that the total OC contents in surface and subsurface sediments are initially different, it is not applicable to use the difference of modern OC contents between surface and subsurface sediments to evaluate the OC degradation proportion. Instead, we applied a more direct method to estimate the proportion of OC degraded during burial (f_{deg}) by the following equation:

$$f_{deg} = Fm_{surface} - Fm_{subsurface} \quad (5)$$

The estimated average f_{deg} values are 11.5% in the high-input regions and 7.5% in the low-input regions, respectively.

Ramped pyrolysis-oxidation (RPO) analysis

Prior to RPO analysis, each grain-size fraction was pretreated with acid rinsing[72]. Specifically, 10 mL of 1 N HCl was added to the sample in a Teflon bottle, which was then agitated and incubated in a water bath at 60°C for 1 h. After centrifugation (1,080 g), the supernatant was removed by pipetting and decanting. To eliminate residual acid, the sample was rinsed three times with 10 mL Milli-Q water following the same agitation and centrifugation steps. The final residues were vacuum-filtered onto pre-combusted GF/F filters using a glass filtration setup, placed in glass Petri dishes, and dried under vacuum for 24 h.

RPO analysis were performed using an Organic and Elemental Carbon (OEC) analyzer (Model 5L-NDIR-O_2, Sunset Laboratory, INC, USA) following the procedure detailed in ref. 73. In brief, the dried sample was weighed and placed in a quartz reactor, where it was subjected to a controlled linear heating ramp from room temperature to 870 °C at 20°C/min. As the sample decomposed, carbon fractions were oxidized to CO_2 in a manganese dioxide combustion furnace, and the resulting CO_2 was continuously quantified.

The evolved CO_2 signal from RPO analysis was deconvolved into three Gaussian-distributed components corresponding to distinct thermal stability windows (C_1, C_2, and C_3). The fitting was performed using non-linear least squares regression in OriginPro employing the Peak Fit (Gaussian) module. Each thermogram was modeled using three Gaussian peaks superimposed on a constant baseline, with peak centers typically located around ~174°C (C_1), ~343°C (C_2), and ~534°C (C_3). These thermal components represent OC pools with progressively increasing resistance to thermal decomposition. Peak fitting achieved generally high goodness-of-fit, with reduced chi-square values < 1 and $R^2 > 0.99$. In addition to grain-size-specific profiles, a weight-normalized RPO reconstruction was further performed using the dry weight proportion of each grain-size fraction to produce integrated thermal profiles and component quantification for the bulk sediment (Fig. S7).

Subduction carbon flux estimation

To evaluate the fate of organic carbon in subduction zones, we conducted a comparative flux analysis across circum-Pacific subduction margins. OC degradation and pyrolysis data from high-input sites in the Japan Trench were used to parameterize fluxes in accretionary margins,

whereas data from low-input sites were applied to erosive margins. We first adopted published OC delivery fluxes to the trench axis from ref. 56., denoted as the amount of OC delivered to trench (Mt/yr), and then estimate the OC flux alteration by different processes step-wise.

To estimate OC loss via early degradation, the average f_{deg} (defined in previous section) from "high-input" and "low input" environments are representing accretionary and erosive margins, respectively. This yields the amount of OC degraded, calculated as:

$$OC_{Degraded} = OC_{Delivered} \times f_{deg} \quad (6)$$

In accretionary margins, the remaining OC is partially retained within the accretionary wedge. This amount of OC stored in accretionary wedge is estimated using the residual OC after degradation by the accretion efficiency:

$$OC_{Acc} = (OC_{Delivered} - OC_{Degraded}) \times f_{acc} \quad (7)$$

Where f_{acc} is the accretion efficiency (%) from ref. 56.

The OC not degraded or stored is then subject to thermal alteration during subduction. To estimate the amount of OC pyrolyzed, we used the proportion of thermally labile carbon (C_1) relative to the sum of the more stable pools ($C_2 + C_3$), based on weight-normalized RPO thermograms (Fig. S6):

$$OC_{Pyrolyzed} = (OC_{Delivered} - OC_{Degraded} - OC_{Acc}) \times f_{pyr} \quad (8)$$

Where f_{pyr} is calculated based on the relative proportion of C_1 thermal fraction:

$$f_{pyr} = A_{C1}/(A_{C2} + A_{C3}) \quad (9)$$

Where A_{C1}, A_{C2} and A_{C3} are the fitted areas of C_1, C_2 and C_3 thermal fractions, respectively (separated by RPO, Fig. S7). The calculated f_{pyr} for accretionary (represented by high-input regions) and erosive (represented by low-input regions) margins are 8.2% and 3.8%, respectively.

Finally, the amount of OC subducted is determined by removing the degraded, stored, and pyrolyzed fractions from the total OC delivered to the trench:

$$OC_{Subducted} = OC_{Delivered} - OC_{Degraded} - OC_{Acc} - OC_{Pyrolyzed} \quad (10)$$

All calculated fluxes are reported in Table 1.

We also present the proportions of degraded, accreted, pyrolyzed and subducted carbon fluxes relative to OC input flux in global trenches in Fig. 4. The pyrolyzation proportions shown in Fig. 4 represent the globally integrated values for accretionary and erosive margins, calculated as the total amount of OC pyrolyzed across all trenches within each margin type divided by the total OC input flux. This yields values of 5.6% for accretionary margins and 3.5% for erosive margins.

Data availability

All data generated in this study are provided in the Supplementary Information and Source Data file. The data used to generate the figures in this study are available in Figshare database[75] (https://doi.org/10.6084/m9.figshare.31419185). Source data are provided with this paper.

References

1. LaRowe, D. E. et al. The fate of organic carbon in marine sediments - New insights from recent data and analysis. *Earth-Sci. Rev.* **204**, 103146 (2020).
2. Eglinton, T. I. & Repeta, D. J. Organic Matter in the Contemporary Ocean. in *Treatise on Geochemistry: Marine Organic Geochemistry* vol. 6 145–180 (Elsevier, 2003).
3. Plank, T. & Manning, C. E. Subducting carbon. *Nature* **574**, 343–352 (2019).
4. Bao, R. et al. Widespread dispersal and aging of organic carbon in shallow marginal seas. *Geology* **44**, 791–794 (2016).
5. Zhao, B. et al. The remineralization of sedimentary organic carbon in different sedimentary regimes of the Yellow and East China Seas. *Chem. Geol.* **495**, 104–117 (2018).
6. Blair, N. E. & Aller, R. C. The fate of terrestrial organic carbon in the marine environment. *Ann. Rev. Mar. Sci.* **4**, 401–423 (2012).
7. Bao, R. et al. Influence of hydrodynamic processes on the fate of sedimentary organic matter on continental margins. *Glob. Biogeochem. Cycles* **32**, 1420–1432 (2018).
8. Jørgensen, B. B., Wenzhöfer, F., Egger, M. & Glud, R. Sediment oxygen consumption: Role in the global marine carbon cycle. *Earth-Sci. Rev.* **228**, 103987 (2022).
9. Komada, T. et al. Dissolved organic carbon dynamics in anaerobic sediments of the Santa Monica Basin. *Geochim. Cosmochim. Acta* **110**, 253–273 (2013).
10. Zabel, M. et al. High carbon mineralization rates in subseafloor hadal sediments—result of frequent mass wasting. *Geochem. Geophys. Geosyst.* **23**, e2022GC010502 (2022).
11. Xu, Y. et al. Distribution, source, and burial of sedimentary organic carbon in kermadec and atacama trenches. *J. Geophys. Res. Biogeosci.* **126**, e2020JG006189 (2021).
12. Xu, Y. et al. Glycerol dialkyl glycerol tetraethers in surface sediments from three Pacific trenches: Distribution, source and environmental implications. *Org. Geochem.* **147**, 104079 (2020).
13. Flores, E. et al. Bacterial and eukaryotic intact polar lipids point to in situ production as a key source of labile organic matter in hadal surface sediment of the Atacama Trench. *Biogeosciences* **19**, 1395–1420 (2022).
14. Reece, J. K., Dorrell, R. M. & Straub, K. M. Circulation of hydraulically ponded turbidity currents and the filling of continental slope minibasins. *Nat. Commun.* **15**, 2075 (2024).
15. Azpiroz-Zabala, M. et al. Newly recognized turbidity current structure can explain prolonged flushing of submarine canyons. *Sci. Adv.* **3**, e1700200 (2017).
16. Oguri, K. et al. Hadal disturbance in the Japan Trench induced by the 2011 Tohoku-Oki earthquake. *Sci. Rep.* **3**, 1915 (2013).
17. Tegler, L. A. et al. Distribution and Drivers of Organic Carbon Sedimentation Along the Continental Margins. *AGU Adv.* **5**, 1–22 (2024).
18. Arndt, S. et al. Quantifying the degradation of organic matter in marine sediments: A review and synthesis. *Earth-Sci. Rev.* **123**, 53–86 (2013).
19. Chu, M. et al. Earthquake-enhanced dissolved carbon cycles in ultra-deep ocean sediments. *Nat. Commun.* **14**, 5427 (2023).
20. Zhang, X. et al. Metagenomics reveals microbial diversity and metabolic potentials of seawater and surface sediment from a hadal biosphere at the Yap trench. *Front. Microbiol.* **9**, 1–15 (2018).
21. Kioka, A. et al. Event Stratigraphy in a Hadal Oceanic Trench: The Japan Trench as Sedimentary Archive Recording Recurrent Giant Subduction Zone Earthquakes and Their Role in Organic Carbon Export to the Deep Sea. *Front. Earth Sci.* **7**, 319 (2019).
22. Ikehara, K. et al. Characteristics and distribution of the event deposits induced by the 2011 Tohoku-oki earthquake and tsunami offshore of Sanriku and Sendai, Japan. *Sediment. Geol.* **411**, 105791 (2021).
23. Ishiwatari, R. et al. Source of organic matter in sinking particles in the Japan Trench: Molecular composition and carbon isotopic analyses. in *Dynamics and Characterization of Marine Organic Matter* 141–168 (2000).
24. Bao, R. et al. Tectonically-triggered sediment and carbon export to the Hadal zone. *Nat. Commun.* **9**, 121 (2018).

25. Schwestermann, T. et al. Multivariate statistical and multiproxy constraints on earthquake-triggered sediment remobilization processes in the central Japan trench. *Geochem. Geophys. Geosyst.* **21**, e2019GC008861 (2020).
26. Seibert, C., Mchugh, C., Paola, C., Seeber, L. & Tucker, J. Surficial sediment remobilization by shear between sediment and water above tsunamigenic megathrust ruptures: Experimental study. *Earth Surf. Dyn.* **13**, 341–348 (2025).
27. McHugh, C. M. et al. Offshore sedimentary effects of the 12 January 2010 Haiti earthquake. *Geology* **39**, 723–726 (2011).
28. Talling, P. J. et al. The global turbidity current pump and its implications for organic carbon cycling. *Ann. Rev. Mar. Sci.* **16**, 105–133 (2024).
29. Talling, P. J. et al. Detailed monitoring reveals the nature of submarine turbidity currents. *Nat. Rev. Earth Environ.* **4**, 642–658 (2023).
30. Underwood, M. B. Composition of fine-grained sediment in the Hikurangi Trough: Evidence for intermingling among axial gravity flows, transverse gravity flows and margin-parallel ocean currents. *Sedimentology* **70**, 828–864 (2023).
31. Pouderoux, H., Proust, J. N., Lamarche, G., Orpin, A. & Neil, H. Postglacial (after 18ka) deep-sea sedimentation along the Hikurangi subduction margin (New Zealand): Characterisation, timing and origin of turbidites. *Mar. Geol.* **295–298**, 51–76 (2012).
32. Thomsen, L. & Gust, G. Sediment erosion thresholds and characteristics of resuspended aggregates on the western European continental margin. *Deep. Res. Part I Oceanogr. Res. Pap.* **47**, 1881–1897 (2000).
33. McCave, I. N. & Hall, I. R. Size sorting in marine muds: Processes, pitfalls, and prospects for paleoflow-speed proxies. *Geochem. Geophys. Geosyst.* **7**, Q10N05 (2006).
34. Paradis, S. et al. The modern ocean sediment archive and inventory of carbon (MOSAIC): Version 2.0. *Earth Syst. Sci. Data* **15**, 4105–4125 (2023).
35. Bao, R., Blattmann, T. M., McIntyre, C., Zhao, M. & Eglinton, T. I. Relationships between grain size and organic carbon 14C heterogeneity in continental margin sediments. *Earth Planet. Sci. Lett.* **505**, 76–85 (2019).
36. Nishida, N., Ito, M., Inoue, A. & Takizawa, S. Clay fabric of fluid-mud deposits from laboratory and field observations: Potential application to the stratigraphic record. *Mar. Geol.* **337**, 1–8 (2013).
37. Ashi, J., Sawada, R., Omura, A. & Ikehara, K. Accumulation of an earthquake-induced extremely turbid layer in a terminal basin of the Nankai accretionary prism. *Earth Planets Sp.* **66**, 1–9 (2014).
38. Strasser, M. et al. Japan Trench event stratigraphy: First results from IODP giant piston coring in a deep-sea trench to advance subduction zone paleoseismology. *Mar. Geol.* **477**, 107387 (2024).
39. Hovikoski, J. et al. Bioturbation in the hadal zone. *Nat. Commun.* **16**, 1401 (2025).
40. McHugh, C. M. et al. Sedimentary signatures of large earthquakes along the submerged Enriquillo–Plantain Garden transpressional plate boundary, northern Caribbean. *Geology* **52**, 769–773 (2024).
41. Luo, M. et al. Rapid burial and intense degradation of organic matter drive active silicate weathering in the subsurface sediments of the ocean's deepest realm. *Geology* **53**, 636–641 (2025).
42. Usami, K., Ikehara, K., Kanamatsu, T. & McHugh, C. M. Supercycle in great earthquake recurrence along the Japan Trench over the last 4000 years. *Geosci. Lett.* **5**, 11 (2018).
43. Chui, Y. et al. Radiocarbon chronology of sediments with implications for climatic events in Lop Nur, NW China. *J. Asian Earth Sci.* **263**, 106024 (2024).
44. Licht, K. J., Cunningham, W. L., Andrews, J. T., Domack, E. W. & Jennings, A. E. Establishing chronologies from acid-insoluble organic14C dates on antarctic (Ross Sea) and arctic (North Atlantic) marine sediments. *Polar Res.* **17**, 203–216 (1998).
45. Rivera-Araya, M., Rowe, C., Levchenko, V., Ulm, S. & Bird, M. I. A radiocarbon chronology for Sanamere Lagoon, Cape York Peninsula, using multiple organic fractions. *Quat. Geochronol.* **70**, 101273 (2022).
46. Kioka, A. et al. Megathrust earthquake drives drastic organic carbon supply to the hadal trench. *Sci. Rep.* **9**, 1553 (2019).
47. Ikehara, K. et al. Spatial variability in sediment lithology and sedimentary processes along the Japan Trench: Use of deep-sea turbidite records to reconstruct past large earthquakes. *Geol. Soc. Spec. Publ.* **456**, 75–89 (2018).
48. Schwestermann, T. et al. Event-dominated transport, provenance, and burial of organic carbon in the Japan Trench. *Earth Planet. Sci. Lett.* **563**, 116870 (2021).
49. Chu, M. et al. Removal of dissolved organic carbon in the West Pacific hadal zones. *Nat. Commun.* **16**, 733 (2025).
50. Chu, M. et al. Earthquake-induced redistribution and reburial of microbes in the hadal trenches. *Innov. Geosci.* **1**, 100027 (2023).
51. Suzuki, K., Yamamoto, M., Rosenheim, B. E., Omori, T. & Polyak, L. New radiocarbon estimation method for carbonate-poor sediments: A case study of ramped pyrolysis 14C dating of postglacial deposits from the Alaskan margin, Arctic Ocean. *Quat. Geochronol.* **66**, 101215 (2021).
52. Hemingway, J. D. et al. Microbial oxidation of lithospheric organic carbon in rapidly eroding tropical mountain soils. *Science* **360**, 209–212 (2018).
53. Hemingway, J. D., Rothman, D. H., Rosengard, S. Z. & Galy, V. V. Technical note: An inverse method to relate organic carbon reactivity to isotope composition from serial oxidation. *Biogeosciences* **14**, 5099–5114 (2017).
54. Han, D., Park, Y. H. & Lee, C. Pressure-driven processes explain the decreasing magnetization of the subducting oceanic crust in the Japan Trench. *Commun. Earth Environ.* **4**, 1–10 (2023).
55. Burdige, D. J. Temperature dependence of organic matter remineralization in deeply-buried marine sediments. *Earth Planet. Sci. Lett.* **311**, 396–410 (2011).
56. Clift, P. D. A revised budget for Cenozoic sedimentary carbon subduction. *Rev. Geophys.* **55**, 97–125 (2017).
57. Clift, P. & Vannucchi, P. Controls on tectonic accretion versus erosion in subduction zones: Implications for the origin and recycling of the continental crust. *Rev. Geophys.* **42**, RG2001 (2004).
58. Lallemand, S., Peyret, M., Arcay, D. & Heuret, A. Accretion versus erosion and sediment transfer balance near the subduction interface. *Comptes Rendus - Geosci.* **356**, 27–51 (2024).
59. Kallmeyer, J. et al. Sulfate reduction rates in Peru Margin sediments: From 1 cm to 100 m below seafloor. *Geochim. Cosmochim. Acta* **399**, 111–124 (2025).
60. Schauberger, C. et al. Spatial variability of prokaryotic and viral abundances in the Kermadec and Atacama Trench regions. *Limnol. Oceanogr.* **66**, 2095–2109 (2021).
61. Saino, T. et al. Short term variability of particle fluxes and its relation to variability in sea surface temperature and chlorophyll a field detected by ocean color and temperature scanner (OCTS) off Sanriku, Northwestern North Pacific in the Spring of 1997. *J. Oceanogr.* **54**, 583–592 (1998).
62. Debret, B. et al. High-pressure synthesis and storage of solid organic compounds in active subduction zones. *Sci. Adv.* **8**, eabo2397 (2022).
63. Giuliani, A. et al. Perturbation of the deep-Earth carbon cycle in response to the Cambrian Explosion. *Sci. Adv.* **8**, eabj1325 (2022).
64. DeMets, C., Gordon, R. G. & Argus, D. F. Geologically current plate motions. *Geophys. J. Int.* **181**, 1–80 (2010).
65. McHugh, C. M. et al. Isotopic and sedimentary signature of megathrust ruptures along the Japan subduction margin. *Mar. Geol.* **428**, 106283 (2020).

66. Ikehara, K. et al. Documenting large earthquakes similar to the 2011 Tohoku-oki earthquake from sediments deposited in the Japan Trench over the past 1500 years. *Earth Planet. Sci. Lett.* **445**, 48–56 (2016).
67. Nakamura, Y. et al. Incoming plate structure at the Japan Trench subduction zone revealed in densely spaced reflection seismic profiles. *Prog. Earth Planet. Sci.* **10**, 45 (2023).
68. Strasser, M., Ikehara, K., Everest, J. & Scientists, E. 386. *Japan Trench Paleoseismology*. *Proceedings of the International Ocean Discovery Program*. vol. 386 (International Ocean Discovery Program, 2023).
69. Bao, R., McNichol, A. P., McIntyre, C. P., Xu, L. & Eglinton, T. I. Dimensions of radiocarbon variability within sedimentary organic matter. *Radiocarbon* **60**, 775–790 (2018).
70. Longworth, B. E., Von Reden, K. F., Long, P. & Roberts, M. L. A high output, large acceptance injector for the NOSAMS Tandetron AMS system. *Nucl. Instrum. Methods Phys. Res. Sect. B Beam Interact. Mater.* **361**, 211–216 (2015).
71. Chu, M., Zhao, M., Eglinton, T. I. & Bao, R. Differentiating the causes of aged organic carbon in marine sediments. *Geophys. Res. Lett.* **49**, e2021GL096912 (2022).
72. Bao, R., McNichol, A. P., Hemingway, J. D., Lardie Gaylord, M. C. & Eglinton, T. I. Influence of different acid treatments on the radiocarbon content spectrum of sedimentary organic matter determined by RPO/accelerator mass spectrometry. *Radiocarbon* **61**, 395–413 (2018).
73. Wu, W. et al. An approach for carbon content measurement in marine sediment: Application of organic and elemental carbon analyzer. *Mar. Environ. Res.* **188**, 106000 (2023).
74. Ikehara, K., Usami, K. & Kanamatsu, T. Repeated occurrence of surface-sediment remobilization along the landward slope of the Japan Trench by great earthquakes. *Earth, Planets Sp.* **72**, 114 (2020).
75. Chu, M. & Bao, R. Organic carbon content and isotope compositions of the Japan Trench sediments collected by IODP 386.xlsx. figshare. Dataset. https://doi.org/10.6084/m9.figshare.31419185 (2026).
76. Tozer, B. et al. Global bathymetry and topography at 15 arc sec: SRTM15. *Earth Space Sci.* **6**, 1847–1864 (2019).
77. Wessel, P. et al. The generic mapping tools version 6. *Geochem., Geophys. Geosyst.* **20**, 5556–5564 (2019).
78. Schlitzer, Reiner. Ocean Data View, odv.awi.de (2023).

Acknowledgements

This research used samples and data provided by IODP. We thank the IODP 386 crew and Science Party for assisting with sample preparation and measurement, and Lihua Dong and Shen Li for technical help. This research is supported by National Natural Science Foundation of China (42525604, R.B.), the National Key R&D Program of China (2025YFF0516900 & 2025YFF0516903, R.B.), National Natural Science Foundation of China (42450135, 92058207, R.B.), China Postdoctoral Science Foundation (2025M780835, M.C.), and the Fundamental Research Funds for the Central Universities (202042010, R.B.).

Author contributions

R.B. and M.C. designed this work with supervision from M.S. and K.I.M.C., and K.L. conducted sample measurements. M.C., R.B., Z.C., T.R., M.K., M.Z., and C.M. contributed to data collection, analysis, and visualization. M.C. and R.B. drafted the figures and wrote the original draft. M.C., Z.C., T.R., M.K., M.Z., C.M., M.S., K.I. and R.B. contributed to the interpretation of data and the editing of the manuscript.

Competing interests

The authors declare no competing interests.

Additional information

Supplementary information The online version contains supplementary material available at https://doi.org/10.1038/s41467-026-72049-9.

Correspondence and requests for materials should be addressed to Rui Bao.

Peer review information *Nature Communications* thanks Edgart Flores and the other, anonymous, reviewer(s) for their contribution to the peer review of this work. A peer review file is available.

Reprints and permissions information is available at http://www.nature.com/reprints

Publisher's note Springer Nature remains neutral with regard to jurisdictional claims in published maps and institutional affiliations.

Open Access This article is licensed under a Creative Commons Attribution-NonCommercial-NoDerivatives 4.0 International License, which permits any non-commercial use, sharing, distribution and reproduction in any medium or format, as long as you give appropriate credit to the original author(s) and the source, provide a link to the Creative Commons licence, and indicate if you modified the licensed material. You do not have permission under this licence to share adapted material derived from this article or parts of it. The images or other third party material in this article are included in the article's Creative Commons licence, unless indicated otherwise in a credit line to the material. If material is not included in the article's Creative Commons licence and your intended use is not permitted by statutory regulation or exceeds the permitted use, you will need to obtain permission directly from the copyright holder. To view a copy of this licence, visit http://creativecommons.org/licenses/by-nc-nd/4.0/.

© The Author(s) 2026